arXiv:2002.07934v1 [nucl-ex] 19 Feb 2020

A sensitivity study of the primary correlators used to characterize chiral-magnetically-driven charge separation

Niseem Magdy,[1,*] Mao-Wu Nie,[2,3] Guo-Liang Ma,[4,5,†] and Roy A. Lacey[6,‡]

[1] *Department of Physics, University of Illinois at Chicago, Chicago, Illinois 60607, USA*
[2] *Institute of Frontier and Interdisciplinary Science, Shandong University, Qingdao, Shandong, 266237, China*
[3] *Key Laboratory of Particle Physics and Particle Irradiation, Ministry of Education, Shandong University, Qingdao, Shandong, 266237, China*
[4] *Key Laboratory of Nuclear Physics and Ion-beam Application (MOE), Institute of Modern Physics, Fudan University, Shanghai 200433, China*
[5] *Shanghai Institute of Applied Physics, Chinese Academy of Sciences, Shanghai 201800, China*
[6] *Depts. of Chemistry & Physics, Stony Brook University, Stony Brook, New York 11794, USA*

(Dated: October 26, 2021)

A Multi-Phase Transport (AMPT) model is used to study the detection sensitivity of two of the primary correlators – $\Delta\gamma$ and R_{Ψ_2} – employed to characterize charge separation induced by the Chiral Magnetic Effect (CME). The study, performed relative to several event planes for different input "CME signals", indicates a detection threshold for the fraction $f_{\rm CME} = \Delta\gamma_{\rm CME}/\Delta\gamma$, which renders the $\Delta\gamma$-correlator insensitive to values of the Fourier dipole coefficient $a_1 \lesssim 2.5\%$, that is larger than the purported signal(signal difference) for ion-ion(isobaric) collisions. By contrast, the R_{Ψ_2} correlator indicates concave-shaped distributions with inverse widths ($\sigma^{-1}_{\rm R_{\Psi_2}}$) that are linearly proportional to a_1, and independent of the character of the event plane used for their extraction. The sensitivity of the R_{Ψ_2} correlator to minimal CME-driven charge separation in the presence of realistic backgrounds, could aid better characterization of the CME in heavy-ion collisions.

PACS numbers: 25.75.-q, 25.75.Gz, 25.75.Ld

Ion-Ion collisions at both the Relativistic Heavy Ion Collider (RHIC) and the Large Hadron Collider (LHC) create hot expanding fireballs of quark-gluon plasma (QGP) in the background of a strong magnetic field [1–3]. Topologically nontrivial sphaleron transitions [via the axial anomaly] [4–6] can induce different densities of right- and left-handed quarks in the plasma fireballs, resulting in a quark electric current along the $\vec{B}$-field. This phenomenon of the generation of a quark electric current ($\vec{J}_Q$) in the presence of a magnetic field is termed the chiral magnetic effect (CME) [7, 8]:

$$\vec{J}_Q = \sigma_5 \vec{B}, \quad \sigma_5 = \mu_5 \frac{Q^2}{4\pi^2}, \tag{1}$$

where, σ_5 is the chiral magnetic conductivity, μ_5 is the chiral chemical potential that quantifies the axial charge asymmetry or imbalance between right- and left-handed quarks in the plasma, and Q is the electric charge [8–11].

Full characterization of the CME, which manifests experimentally as the separation of electrical charges along the $\vec{B}$-field [7, 8], can give fundamental insight on anomalous transport and the interplay of chiral symmetry restoration, axial anomaly and gluon topology in the QGP [12–16].

Charge separation stems from the fact that the CME preferentially drives charged particles, originating from the same "P-odd domain", along or opposite to the $\vec{B}$-field depending on their charge. This separation can be quantified via measurements of the first P-odd sine term a_1, in the Fourier decomposition of the charged-particle azimuthal distribution [17]:

$$\frac{dN^{\rm ch}}{d\phi} \propto [1 + 2\sum_n v_n \cos(n\Delta\phi) + a_n \sin(n\Delta\phi) + ...] \tag{2}$$

where $\Delta\phi = \phi - \Psi_{\rm RP}$ gives the particle azimuthal angle with respect to the reaction plane (RP) angle, and v_n and a_n denote the coefficients of P-even and P-odd Fourier terms, respectively. A direct measurement of the P-odd coefficients a_n, is not possible due to the strict global $\mathcal{P}$ and $\mathcal{CP}$ symmetry of QCD. However, their fluctuation and/or variance $\tilde{a}_n = \langle a_n^2 \rangle^{1/2}$ can be measured with suitable correlators.

The CME-driven charge separation is small because only a few particles from the same P-odd domain are correlated. Moreover, both the initial axial charge and the time evolution of the magnetic field (c.f. Eq. 1) are unconstrained theoretically, and it is uncertain whether an initial CME-driven charge separation could survive the signal-reducing effects of the reaction dynamics, and still produce a signal above the detection threshold. Besides, it is uncertain whether a charge separation that survives the expansion dynamics would still be discernible in the presence of the well-known background correlations which contribute and complicate the measurement of CME-driven charge separation [14, 18–22]. Thus, the correlators used to characterize the CME, not only need to suppress background-driven charge-dependent correlations, such as the ones from resonance decays, charge ordering in jets, etc., but should also be sensitive to small charge separation signals in the presence of these

backgrounds. The latter requirement is especially important for ongoing measurements [at RHIC] designed to detect the small signal difference between the Ru+Ru and Zr+Zr isobars [23].

In this work we use the AMPT model [24] with varying amounts of input charge separation ΔS, characterized by the partonic dipole term a_1, to study the detection sensitivity of the $\Delta\gamma$ and the $R_{\Psi_2}(\Delta S)$ correlators. The model is known to give a good representation of the experimentally measured particle yields, spectra, flow, etc.,[24–29]. Therefore, it provides a realistic estimate of both the magnitude and the properties of the background-driven charge separation one might encounter in the data sets collected at RHIC and the LHC.

For these sensitivity tests, we simulated Au+Au collisions at $\sqrt{s_{\rm NN}}$ = 200 GeV with the new version of the AMPT model that incorporates string melting and local charge conservation. There are four primary ingredients for each of these collisions: (i) an initial-state, (ii) a parton cascade phase, (iii) a hadronization phase in which partons are converted to hadrons, and (iv) a hadronic re-scattering phase prior to kinetic freeze-out. The initial-state mainly simulates the spatial and momentum distributions of minijet partons from QCD hard processes and soft string excitations as encoded in the HIJING model [30, 31]. The parton cascade takes account of the strong interactions among partons through elastic partonic collisions controlled by a parton interaction cross section [32]. Hadronization, or the conversion from partonic to hadronic matter, is simulated via a coalescence mechanism. Subsequent to hadronization, the ART model is used to simulate baryon-baryon, baryon-meson and meson-meson interactions [33].

A formal mechanism for the CME is not implemented in AMPT. However, modifications can be made to the model to mimic CME-induced charge separation [34] by switching the p_y values of a fraction of the downward moving u ($\bar{d}$) quarks with those of the upward moving $\bar{u}$ (d) quarks to produce a net charge-dipole separation in the initial-state. Here, the x axis is along the direction of the impact parameter b, the z axis points along the beam direction, and the y axis is perpendicular to the x and z directions, *i.e*, the direction of the proxy $\vec{B}$-field. The strength of the proxy CME signal is regulated by the fraction f_0 of the initial input charge separation [34, 35]:

$$f_0 = \frac{N^{+(-)}_{\uparrow(\downarrow)} - N^{+(-)}_{\downarrow(\uparrow)}}{N^{+(-)}_{\uparrow(\downarrow)} + N^{+(-)}_{\downarrow(\uparrow)}}, \quad f_0 = \frac{4}{\pi} a_1 \tag{3}$$

where N is the number of a given species of quarks, "$+$" and "$-$" denote positive and negative charges, respectively, and $\uparrow$ and $\downarrow$ represent the directions along and opposite to that of the y axis. Eq. 3 also shows that the fraction f_0, is related to the P-odd dipole term a_1, defined in Eq. 2. Note that this initial partonic charge separation a_1, is different from the final hadrons' charge separation a_1, often referred to in the literature and implemented in other models. Cross-checks made with the Anomalous-Viscous Fluid Dynamics model [36, 37] suggests that the two are linearly proportional to a very good approximation. Simulated events, generated for a broad set of f_0 values, were analyzed with both the $\Delta\gamma$ and the $R_{\Psi_2}(\Delta S)$ correlators, to evaluate their respective sensitivity as discussed below quantitatively.

The charge-dependent correlator, $\gamma_{\alpha\beta}$ [17] , has been widely used at RHIC [38–44] and the LHC [22, 45] in ongoing attempts to identify and quantify CME-driven charge separation:

$$\gamma_{\alpha\beta} = \left\langle \cos\left(\phi^{(\pm)}_{\alpha} + \phi^{(\pm)}_{\beta} - 2\Psi_2\right)\right\rangle, \quad \Delta\gamma = \gamma_{\beta} - \gamma_{\alpha},$$

where ϕ_α, ϕ_β denote the azimuthal emission angles for like-sign ($++$, $--$) and unlike-sign ($+-$) particle pairs. The question as to whether the experimental measurements for $\Delta\gamma$ indicate the CME, remain inconclusive because of several known sources of background correlations that can account for most, if not all, of the measurements [14, 18–21].

A recent embellishment to the $\Delta\gamma$ correlator is the proposal to leverage the ratios of $\Delta\gamma$ and elliptic flow (v_2) measurements, obtained relative to the reaction plane ($\Psi_{\rm RP}$) and the participant plane ($\Psi_{\rm PP}$)

$$r_1 = \frac{\Delta\gamma(\Psi_{\rm RP})}{\Delta\gamma(\Psi_{\rm PP})}, \quad r_2 = \frac{v_2(\Psi_{\rm RP})}{v_2(\Psi_{\rm PP})}, \tag{4}$$

to simultaneously constrain the CME and background (Bkg) contributions to $\Delta\gamma$ [46, 47]:

$$\begin{aligned} \Delta\gamma(\Psi_{\rm PP}) &= \Delta\gamma_{\rm CME}(\Psi_{\rm PP}) + \Delta\gamma_{\rm Bkg}(\Psi_{\rm PP}), \\ \Delta\gamma(\Psi_{\rm RP}) &= \Delta\gamma_{\rm CME}(\Psi_{\rm RP}) + \Delta\gamma_{\rm Bkg}(\Psi_{\rm RP}), \end{aligned} \tag{5}$$

and

$$\begin{aligned} \Delta\gamma_{\rm CME}(\Psi_{\rm PP}) &= r_2 \times \Delta\gamma_{\rm CME}(\Psi_{\rm RP}), \\ \Delta\gamma_{\rm Bkg}(\Psi_{\rm RP}) &= r_2 \times \Delta\gamma_{\rm Bkg}(\Psi_{\rm PP}), \end{aligned} \tag{6}$$

where it is assumed that the CME is proportional to the magnetic field squared and the background (Bkg) is proportional to v_2. The fraction of the measured $\Delta\gamma(\Psi_{\rm PP})$, attributable to the CME, can then be estimated as [46];

$$\begin{aligned} f_{\rm CME} &= \Delta\gamma_{\rm CME}(\Psi_{\rm PP})/\Delta\gamma(\Psi_{\rm PP}) = f_1/f_2, \\ \text{where} \quad f_1 &= \frac{r_1}{r_2} - 1 \quad \text{and} \quad f_2 = \frac{1}{r_2^2} - 1. \end{aligned} \tag{7}$$

The underlying idea behind the constraints expressed in Eqs. 4 - 7 is that the v_2-driven background is more strongly correlated with $\Psi_{\rm PP}$ [determined by the maximal particle density in the elliptic azimuthal anisotropy and the beam axis], than with $\Psi_{\rm RP}$ [determined by the impact vector $\vec{b}$ and the beam direction]. By contrast, the $\vec{B}$-field, which drives the CME, behaves oppositely – weaker correlation with $\Psi_{\rm PP}$ and stronger correlation

with $\Psi_{\rm RP}$. We will employ this new method of leveraging the measurements of r_1 and r_2 to extract $f_{\rm CME}$ from AMPT events as discussed below.

The operational details of the construction and the response of the $R_{\Psi_m}(\Delta S)$ correlator is described in Refs. [48] and [49]. It is constructed for each event plane Ψ_m, as the ratio:

$$R_{\Psi_m}(\Delta S) = C_{\Psi_m}(\Delta S)/C^{\perp}_{\Psi_m}(\Delta S),\ m = 2, 3, \quad (8)$$

where $C_{\Psi_m}(\Delta S)$ and $C^{\perp}_{\Psi_m}(\Delta S)$ are correlation functions that quantify charge separation ΔS, parallel and perpendicular (respectively) to the $\vec{B}$-field. $C_{\Psi_2}(\Delta S)$ measures both CME- and backgrond-driven charge separation while $C^{\perp}_{\Psi_2}(\Delta S)$ measures only background-driven charge separation. The absence of a strong correlation between the orientation of the Ψ_3 plane and the $\vec{B}$-field, also renders $C_{\Psi_3}(\Delta S)$ and $C^{\perp}_{\Psi_3}(\Delta S)$ insensitive to a CME-driven charge separation, but not to the background, so it can give crucial additional insight on the relative importance of background-driven and CME-driven charge separation. However, they are not required for the sensitivity studies presented in this work.

The correlation functions used to quantify charge separation parallel to the $\vec{B}$-field, are constructed from the ratio of two distributions [50]:

$$C_{\Psi_m}(\Delta S) = \frac{N_{\rm real}(\Delta S)}{N_{\rm Shuffled}(\Delta S)},\ m = 2, 3, \quad (9)$$

where $N_{\rm real}(\Delta S)$ is the distribution over events, of charge separation relative to the Ψ_m planes in each event:

$$\Delta S = \left\langle S_p^{h+} \right\rangle - \left\langle S_n^{h-} \right\rangle, \quad (10)$$

$$\Delta S = \frac{\sum_1^p \sin(\frac{m}{2}\Delta\varphi_m)}{p} - \frac{\sum_1^n \sin(\frac{m}{2}\Delta\varphi_m)}{n}, \quad (11)$$

where n and p are the numbers of negatively- and positively charged hadrons in an event, $\Delta\varphi_m = \phi - \Psi_m$ and ϕ is the azimuthal emission angle of the charged hadrons. The $N_{\rm Shuffled}(\Delta S)$ distribution is similarly obtained from the same events, following random reassignment (shuffling) of the charge of each particle in an event. This procedure ensures identical properties for the numerator and the denominator in Eq. 9, except for the charge-dependent correlations which are of interest. The correlation functions $C^{\perp}_{\Psi_m}(\Delta S)$, that quantify charge separation perpendicular to the $\vec{B}$-field, are constructed with the same procedure outlined for $C_{\Psi_m}(\Delta S)$, but with Ψ_m replaced by $\Psi_m + \pi/m$, to ensure that a possible CME-driven charge separation does not contribute to $C^{\perp}_{\Psi_m}(\Delta S)$.

The magnitude of the CME-driven charge separation is reflected in the width σ_{Ψ_2} of the concave-shaped distribution for $R_{\Psi_2}(\Delta S)$, which is also influenced by particle number fluctuations and the resolution of Ψ_2. That is, stronger CME-driven signals lead to narrower concave-shaped distributions (smaller widths), which are made broader by particle number fluctuations and poorer event-plane resolutions. The influence of the particle number fluctuations can be minimized by scaling ΔS by the width $\sigma_{\Delta_{\rm Sh}}$ of the distribution for $N_{\rm shuffled}(\Delta S)$ *i.e.*, $\Delta S^{'} = \Delta S/\sigma_{\Delta_{\rm Sh}}$. Similarly, the effects of the event plane resolution can be accounted for by scaling $\Delta S^{'}$ by the resolution factor $\delta_{\rm Res}$, *i.e.*, $\Delta S^{''} = \Delta S^{'} \times \delta_{Res}$, where $\delta_{\rm Res} = \sigma_{Res} \times e^{(1-\sigma_{Res})^2}$ and $\sigma_{\rm Res}$ is the event plane resolution [48].

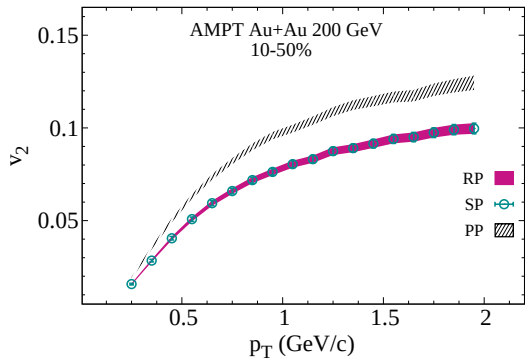


FIG. 1. Comparison of the simulated $v_2(p_T)$ obtained in 10-50% Au+Au collisions ($\sqrt{s_{\rm NN}}$ = 200 GeV) with $\Psi_{\rm RP}$, $\Psi_{\rm SP}$ and $\Psi_{\rm PP}$, see text.

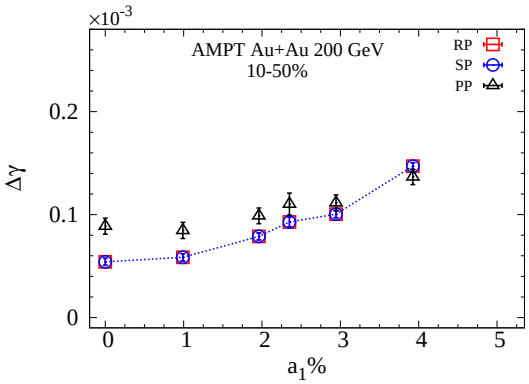


FIG. 2. Comparison of the simulated $\Delta\gamma$ obtained in 10-50% Au+Au collisions ($\sqrt{s_{\rm NN}}$ = 200 GeV) with respect to $\Psi_{\rm RP}$, $\Psi_{\rm SP}$ and $\Psi_{\rm PP}$, for several input charge separation fractions characterized by the P-odd dipole coefficient a_1.

The $10-50\%$ central AMPT events, generated for several input values of charge separation f_0 (cf. Eq. 3), relative to the reaction- $\Psi_{\rm RP}$, spectator- $\Psi_{\rm SP}$ and the participant plane $\Psi_{\rm PP}$, were analyzed to extract $f_{\rm CME}$ via the $\Delta\gamma$ correlator and σ_{Ψ_2} via the $R_{\Psi_2}(\Delta S)$ correlator. Approximately 10^6 events were generated for each value of f_0. The analyses included charged particles with

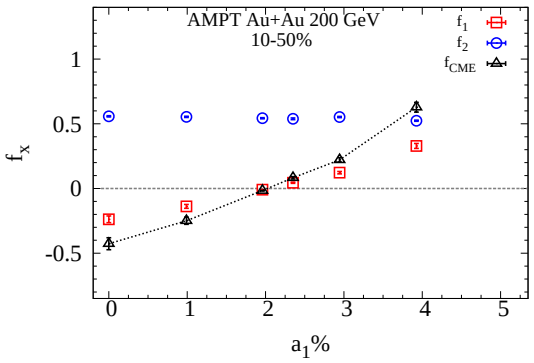


FIG. 3. The dependence of f_1, f_2 and $f_{\rm CME}$ on different input charge separation characterized by the dipole coefficient a_1, see Eqs. 3 and 7. Results are shown for 10-50% central Au+Au ($\sqrt{s_{\rm NN}}$ = 200 GeV) AMPT events.

$|\eta| < 1.0$ and transverse momentum $0.2 < p_T < 2$ GeV/c. To enhance the statistical significance of the measurements, the participant plane $\Psi_{\rm PP}$ was determined with charged hadrons in the range $2.5 < \eta < 4.0$. The charge separation of charged hadrons in $|\eta| < 1.0$ were then measured relative to $\Psi_{\rm PP}$. Representative results are summarized in Figs. 1 - 4.

Figure 1 compares the $v_2(p_T)$ obtained with $\Psi_{\rm RP}$, $\Psi_{\rm SP}$ and $\Psi_{\rm PP}$ for 10-50% Au+Au collisions. It shows the expected similarity between the results for $\Psi_{\rm RP}$ and $\Psi_{\rm SP}$, as well as larger values for $\Psi_{\rm PP}$ that confirm the enhanced fluctuations associated with the participant geometry and consequently, the initial-state eccentricity ε_2. This difference is essential for the procedure outlined in Eqs. 4 - 7.

A similar comparison of the $\Delta\gamma$ results for the three planes is given in Fig. 2. It shows that for $a_1 \lesssim 3\%$, the $\Delta\gamma$ values obtained with $\Psi_{\rm PP}$ are larger than those obtained with $\Psi_{\rm RP}$ and $\Psi_{\rm SP}$; there is also little, if any, difference between the values obtained with $\Psi_{\rm RP}$ and $\Psi_{\rm SP}$ over the full range of the input a_1 values. This latter trend is to be expected since the fluctuation of $\Psi_{\rm SP}$ about $\Psi_{\rm RP}$ is small. For $a_1 \gtrsim 4\%$, the $\Delta\gamma$ values for $\Psi_{\rm RP}$ and $\Psi_{\rm SP}$ become larger than the ones for $\Psi_{\rm PP}$ (not shown in Fig. 2), consistent with a stronger influence from the proxy CME-driven charge separation.

The extracted values of v_2 and $\Delta\gamma$, with respect to $\Psi_{\rm PP}$ and $\Psi_{\rm SP}$ were used to evaluate f_1, f_2 and $f_{\rm CME}$ following the procedure outlined in Eqs. 4 - 7 [46]. Fig. 3 summarizes the a_1 dependence of f_1, f_2 and $f_{\rm CME}$. It indicates a flat f_2, consistent with the expectation that the v_2 fluctuations should be relatively insensitive to the introduction of small a_1 signals. By contrast, f_1 and $f_{\rm CME}$, which are both negative for $a_1 \lesssim 2.5\%$, show an increase with a_1 and become positive for $a_1 \gtrsim 2.5\%$. The negative values observed for $f_{\rm CME}$ suggests that for $a_1 \lesssim 2.5\%$, the correlator is either (i) unable to make the robust distinction between signal and background required to measure the input proxy CME-signal or (ii) the assumptions used to estimate $f_{\rm CME}$ are invalid. Note that $f_{\rm CME}$ is only 0.6 even for a relatively large input signal of $a_1 = 4.0\%$.

The change from negative to positive values for $f_{\rm CME}$ (cf. Fig. 3) suggests a *"turn-on"* a_1 value, below which, the modified $\Delta\gamma$ correlator (cf. Eqs. 4 - 7) is unable to detect a CME-driven signal. This detection threshold could pose a significant limitation for CME detection and characterization with this correlator, because it is comparable to, or larger than the magnitude of the CME-driven charge separation expected in actual experiments. Equally important is the fact that $f_{\rm CME} \leq 0.0$ does not give a robust indication of the absence of a CME signal. The latter could have important implications for the interpretation of current and future $f_{\rm CME}$ measurements.

The sensitivity of the $R_{\Psi_{\rm XX}}(\Delta S)$ (XX = RP, SP, PP) correlator to varying degrees of input CME-driven charge separation (characterized by a_1) was studied using the same AMPT events employed in the leveraged $\Delta\gamma$ study. Figs. 4(a) - (e) show the $R_{\Psi_{\rm XX}}(\Delta S)$ correlator distributions obtained for $10-50\%$ central Au+Au collisions, relative to $\Psi_{\rm RP}$, $\Psi_{\rm SP}$ and $\Psi_{\rm PP}$ for several values of a_1 as indicated. In each of these plots, ΔS is scaled to account for the effects of number fluctuations and event plane resolution as outlined earlier and in Ref. [48].

The concave-shaped distribution, apparent in each panel of Fig. 4 (b) - (e), confirms the input charge separation signal in each case; note the weakly convex-shaped distribution for $a_1 = 0$ in Fig. 4 (a). Note as well that in contrast to the $\Delta\gamma$ correlator, the $R_{\Psi_{\rm XX}}(\Delta S)$ distributions are independent of the plane used to measure them, suggesting that they are less sensitive to the v_2 driven background and their associated fluctuations. The apparent decrease in the widths of these distributions with a_1, also confirm the expected trend.

To quantify the implied signal strengths, we extracted the width $\sigma_{\rm R_{\Psi_2}}$ of the $R_{\Psi_2}(\Delta S)$ distributions obtained for the respective values of a_1. Fig. 4(f) shows the inverse widths $\sigma^{-1}_{\rm R_{\Psi_2}}$ vs. a_1. They indicate an essentially linear dependence on a_1 (note the dotted line fit). Here, it is noteworthy that for $a_1 \lesssim 0.5\%$, significant additional statistics are required to determine $\sigma_{\rm R_{\Psi_2}}$ with good accuracy. These results suggests that the $R_{\Psi_m}(\Delta S)$ correlator not only suppresses background, but is sensitive to very small CME-driven charge separation in the presence of such backgrounds.

In summary, we have used both the $R_{\Psi_2}(\Delta S)$ correlator and an event-plane-leveraged version of the $\Delta\gamma$ correlator to analyze AMPT events with varying degrees of input proxy CME signals. Our sensitivity study indicates a *turn-on* threshold for $f_{\rm CME} = \Delta\gamma_{\rm CME}/\Delta\gamma$, which renders the leveraged $\Delta\gamma$-correlator insensitive to input signals with $a_1 \lesssim 2.5\%$. The magnitude of this detection threshold, which is comparable to that for the purported signal in heavy ion collisions and less than the signal difference for isobaric collisions, could pose significant re-

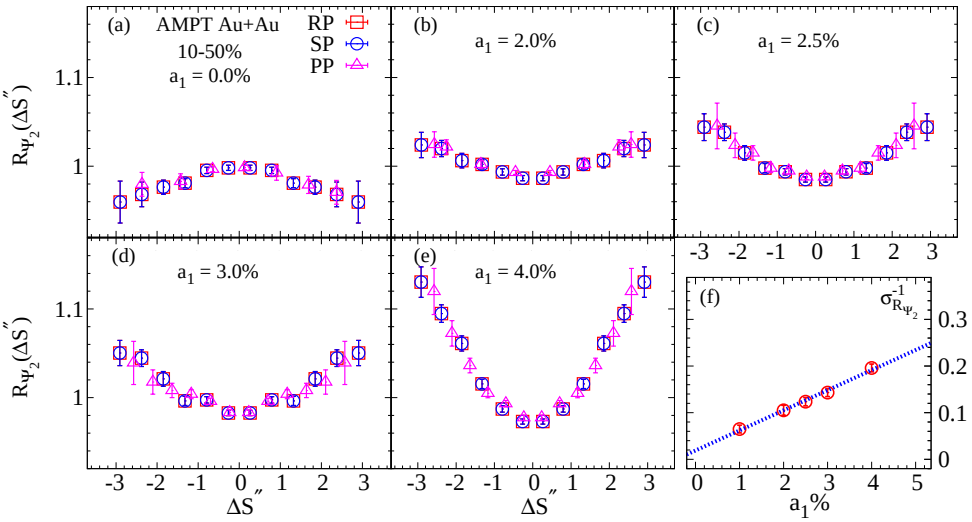


FIG. 4. Comparison of the $R_{\Psi_2}(\Delta S)$ correlators obtained with respect to $\Psi_{\rm RP}$, $\Psi_{\rm SP}$ and $\Psi_{\rm PP}$ for several a_1 values, as indicated, for 10-50% Au+Au collisions at $\sqrt{s_{\rm NN}}$ = 200 GeV (a) - (e). Panel (f) shows the a_1 dependence of the inverse widths $\sigma^{-1}_{\rm R_{\Psi_2}}$, extracted from the $R_{\Psi_2}(\Delta S)$ distributions; the dotted line represents a linear fit.

strictions on its use to detect the CME. By contrast, the a_1-dependent $R_{\Psi_2}(\Delta S)$ correlators indicate inverse widths $\sigma^{-1}_{\rm R_{\Psi_2}}$, that are linearly dependent on a_1, and independent of the character of the event plane ($\Psi_{\rm RP}$, $\Psi_{\rm SP}$ or $\Psi_{\rm PP}$) used for their extraction. These results not only have implications for the interpretation of current and future $f_{\rm CME} = \Delta\gamma_{\rm CME}/\Delta\gamma$ measurements; they further indicate that the $R_{\Psi_2}(\Delta S)$ correlator can provide robust quantification of minimal CME-driven charge separation in the presence of realistic backgrounds, that could aid characterization of the CME in RHIC and LHC collisions.

ACKNOWLEDGMENTS

This research is supported by the US Department of Energy, Office of Science, Office of Nuclear Physics, under contracts DE-FG02-87ER40331.A008 (RL), DE-FG02-94ER40865 (NM) and by the National Natural Science Foundation of China under Grants No. 11890714, No. 11835002, No. 11961131011, and No. 11421505, the Key Research Program of the Chinese Academy of Sciences under Grant No. XDPB09.

* niseemm@gmail.com
† glma@fudan.edu.cn
‡ Roy.Lacey@stonybrook.edu

[1] V. Skokov, A. Yu. Illarionov, and V. Toneev, "Estimate of the magnetic field strength in heavy-ion collisions," Int. J. Mod. Phys. **A24**, 5925–5932 (2009), arXiv:0907.1396 [nucl-th].
[2] L. McLerran and V. Skokov, "Comments About the Electromagnetic Field in Heavy-Ion Collisions," Nucl. Phys. **A929**, 184–190 (2014), arXiv:1305.0774 [hep-ph].
[3] Kirill Tuchin, "Electromagnetic field and the chiral magnetic effect in the quark-gluon plasma," Phys. Rev. **C91**, 064902 (2015), arXiv:1411.1363 [hep-ph].
[4] N. S. Manton, "Topology in the Weinberg-Salam Theory," Phys. Rev. **D28**, 2019 (1983).
[5] Frans R. Klinkhamer and N. S. Manton, "A Saddle Point Solution in the Weinberg-Salam Theory," Phys. Rev. **D30**, 2212 (1984).
[6] Guy D. Moore, "Do we understand the sphaleron rate?" in *Strong and electroweak matter. Proceedings, Meeting, SEWM 2000,* (2000) pp. 82–94, arXiv:hep-ph/0009161 [hep-ph].
[7] Dmitri Kharzeev, "Parity violation in hot QCD: Why it can happen, and how to look for it," Phys. Lett. **B633**, 260–264 (2006), arXiv:hep-ph/0406125.
[8] Kenji Fukushima, Dmitri E. Kharzeev, and Harmen J. Warringa, "The Chiral Magnetic Effect," Phys. Rev. **D78**, 074033 (2008), arXiv:0808.3382 [hep-ph].
[9] Dam T. Son and Piotr Surowka, "Hydrodynamics with Triangle Anomalies," Phys. Rev. Lett. **103**, 191601 (2009), arXiv:0906.5044 [hep-th].
[10] Valentin I. Zakharov, "Chiral Magnetic Effect in Hydrodynamic Approximation," (2012), 10.1007/978-3-642-37305-3-11, [Lect. Notes Phys.871,295(2013)], arXiv:1210.2186 [hep-ph].
[11] Kenji Fukushima, "Views of the Chiral Magnetic Effect," Lect. Notes Phys. **871**, 241–259 (2013), arXiv:1209.5064 [hep-ph].
[12] Guy D. Moore and Marcus Tassler, "The Sphaleron

Rate in SU(N) Gauge Theory," JHEP **02**, 105 (2011), arXiv:1011.1167 [hep-ph].
[13] M. Mace, S. Schlichting, and R. Venugopalan, "Off-equilibrium sphaleron transitions in the Glasma," Phys. Rev. **D93**, 074036 (2016), arXiv:1601.07342 [hep-ph].
[14] Jinfeng Liao, Volker Koch, and Adam Bzdak, "On the Charge Separation Effect in Relativistic Heavy Ion Collisions," Phys. Rev. **C82**, 054902 (2010), arXiv:1005.5380 [nucl-th].
[15] D. E. Kharzeev, J. Liao, S. A. Voloshin, and G. Wang, "Chiral magnetic and vortical effects in high-energy nuclear collisionsA status report," Prog. Part. Nucl. Phys. **88**, 1–28 (2016), arXiv:1511.04050 [hep-ph].
[16] Volker Koch, Soeren Schlichting, Vladimir Skokov, Paul Sorensen, Jim Thomas, Sergei Voloshin, Gang Wang, and Ho-Ung Yee, "Status of the chiral magnetic effect and collisions of isobars," Chin. Phys. **C41**, 072001 (2017), arXiv:1608.00982 [nucl-th].
[17] Sergei A. Voloshin, "Parity violation in hot QCD: How to detect it," Phys. Rev. **C70**, 057901 (2004), arXiv:hep-ph/0406311 [hep-ph].
[18] Fuqiang Wang, "Effects of Cluster Particle Correlations on Local Parity Violation Observables," Phys. Rev. **C81**, 064902 (2010), arXiv:0911.1482 [nucl-ex].
[19] Adam Bzdak, Volker Koch, and Jinfeng Liao, "Azimuthal correlations from transverse momentum conservation and possible local parity violation," (2010), arXiv:1008.4919 [nucl-th].
[20] Soren Schlichting and Scott Pratt, "Charge conservation at energies available at the BNL Relativistic Heavy Ion Collider and contributions to local parity violation observables," Phys. Rev. **C83**, 014913 (2011), arXiv:1009.4283 [nucl-th].
[21] Berndt Muller and Andreas Schafer, "Charge Fluctuations from the Chiral Magnetic Effect in Nuclear Collisions," (2010), arXiv:1009.1053 [hep-ph].
[22] Vardan Khachatryan *et al.* (CMS), "Observation of charge-dependent azimuthal correlations in pPb collisions and its implication for the search for the chiral magnetic effect," Submitted to: Phys. Rev. Lett (2016), arXiv:1610.00263 [nucl-ex].
[23] J. Adam *et al.* (STAR), "Methods for a blind analysis of isobar data collected by the STAR collaboration," (2019), arXiv:1911.00596 [nucl-ex].
[24] Zi-Wei Lin, Che Ming Ko, Bao-An Li, Bin Zhang, and Subrata Pal, "A Multi-phase transport model for relativistic heavy ion collisions," Phys. Rev. **C72**, 064901 (2005), arXiv:nucl-th/0411110 [nucl-th].
[25] Guo-Liang Ma and Zi-Wei Lin, "Predictions for $\sqrt{s_{NN}} = 5.02$ TeV Pb+Pb Collisions from a Multi-Phase Transport Model," Phys. Rev. **C93**, 054911 (2016), arXiv:1601.08160 [nucl-th].
[26] Guo-Liang Ma, "Decomposition of the jet fragmentation function in high-energy heavy-ion collisions," Phys. Rev. **C88**, 021902 (2013), arXiv:1306.1306 [nucl-th].
[27] Guo-Liang Ma, "Medium modifications of jet shapes in Pb+Pb collisions at $\sqrt{s_{\rm NN}}$ = 2.76 TeV within a multiphase transport model," Phys. Rev. **C89**, 024902 (2014), arXiv:1309.5555 [nucl-th].
[28] Adam Bzdak and Guo-Liang Ma, "Elliptic and triangular flow in p+Pb and peripheral Pb+Pb collisions from parton scatterings," Phys. Rev. Lett. **113**, 252301 (2014), arXiv:1406.2804 [hep-ph].
[29] Mao-Wu Nie, Peng Huo, Jiangyong Jia, and Guo-Liang Ma, "Multiparticle azimuthal cumulants in p+Pb collisions from a multiphase transport model," Phys. Rev. **C98**, 034903 (2018), arXiv:1802.00374 [hep-ph].
[30] Xin-Nian Wang and Miklos Gyulassy, "HIJING: A Monte Carlo model for multiple jet production in p p, p A and A A collisions," Phys. Rev. **D44**, 3501–3516 (1991).
[31] Miklos Gyulassy and Xin-Nian Wang, "HIJING 1.0: A Monte Carlo program for parton and particle production in high-energy hadronic and nuclear collisions," Comput. Phys. Commun. **83**, 307 (1994), arXiv:nucl-th/9502021 [nucl-th].
[32] Bin Zhang, "ZPC 1.0.1: A Parton cascade for ultrarelativistic heavy ion collisions," Comput. Phys. Commun. **109**, 193–206 (1998), arXiv:nucl-th/9709009 [nucl-th].
[33] Bao-An Li and Che Ming Ko, "Formation of superdense hadronic matter in high-energy heavy ion collisions," Phys. Rev. **C52**, 2037–2063 (1995), arXiv:nucl-th/9505016 [nucl-th].
[34] Guo-Liang Ma and Bin Zhang, "Effects of final state interactions on charge separation in relativistic heavy ion collisions," Phys. Lett. **B700**, 39–43 (2011), arXiv:1101.1701 [nucl-th].
[35] Ling Huang, Mao-Wu Nie, and Guo-Liang Ma, "Sensitivity analysis of the chiral magnetic effect observables using a multiphase transport model," (2019), arXiv:1906.11631 [nucl-th].
[36] Shuzhe Shi, Yin Jiang, Elias Lilleskov, and Jinfeng Liao, "Anomalous Chiral Transport in Heavy Ion Collisions from Anomalous-Viscous Fluid Dynamics," (2017), arXiv:1711.02496 [nucl-th].
[37] Yin Jiang, Shuzhe Shi, Yi Yin, and Jinfeng Liao, "Quantifying the chiral magnetic effect from anomalous-viscous fluid dynamics," Chin. Phys. **C42**, 011001 (2018), arXiv:1611.04586 [nucl-th].
[38] B. I. Abelev *et al.* (STAR), "Azimuthal Charged-Particle Correlations and Possible Local Strong Parity Violation," Phys. Rev. Lett. **103**, 251601 (2009), arXiv:0909.1739 [nucl-ex].
[39] B. I. Abelev *et al.* (STAR), "Observation of charge-dependent azimuthal correlations and possible local strong parity violation in heavy ion collisions," Phys. Rev. **C81**, 054908 (2010), arXiv:0909.1717 [nucl-ex].
[40] L. Adamczyk *et al.* (STAR), "Fluctuations of charge separation perpendicular to the event plane and local parity violation in $\sqrt{s_{NN}}$ = 200 GeV Au+Au collisions at the BNL Relativistic Heavy Ion Collider," Phys. Rev. **C88**, 064911 (2013), arXiv:1302.3802 [nucl-ex].
[41] L. Adamczyk *et al.* (STAR), "Measurement of charge multiplicity asymmetry correlations in high-energy nucleus-nucleus collisions at $\sqrt{s_{NN}}$ = 200 GeV," Phys. Rev. **C89**, 044908 (2014), arXiv:1303.0901 [nucl-ex].
[42] L. Adamczyk *et al.* (STAR), "Beam-energy dependence of charge separation along the

magnetic field in Au+Au collisions at RHIC," Phys. Rev. Lett. **113**, 052302 (2014), arXiv:1404.1433 [nucl-ex].

[43] Prithwish Tribedy (STAR), "Disentangling flow and signals of Chiral Magnetic Effect in U+U, Au+Au and p+Au collisions," in *Quark Matter 2017, Chicago, Illinois, USA, 2017* (2017) arXiv:1704.03845 [nucl-ex].

[44] Jie Zhao, Hanlin Li, and Fuqiang Wang, "Isolating backgrounds from the chiral magnetic effect," (2017), arXiv:1705.05410 [nucl-ex].

[45] Betty Abelev *et al.* (ALICE), "Charge separation relative to the reaction plane in Pb-Pb collisions at $\sqrt{s_{NN}} = 2.76$ TeV," Phys. Rev. Lett. **110**, 012301 (2013), arXiv:1207.0900 [nucl-ex].

[46] Hao-jie Xu, Jie Zhao, Xiaobao Wang, Hanlin Li, Zi-Wei Lin, Caiwan Shen, and Fuqiang Wang, "Varying the chiral magnetic effect relative to flow in a single nucleus-nucleus collision," Chin. Phys. **C42**, 084103 (2018), arXiv:1710.07265 [nucl-th].

[47] Sergei A. Voloshin, "Estimate of the signal from the chiral magnetic effect in heavy-ion collisions from measurements relative to the participant and spectator flow planes," Phys. Rev. **C98**, 054911 (2018), arXiv:1805.05300 [nucl-ex].

[48] Niseem Magdy, Shuzhe Shi, Jinfeng Liao, N. Ajitanand, and Roy A. Lacey, "A New Correlator to Detect and Characterize the Chiral Magnetic Effect," (2017), arXiv:1710.01717 [physics.data-an].

[49] Niseem Magdy, Shuzhe Shi, Jinfeng Liao, Peifeng Liu, and Roy A. Lacey, "Examination of the observability of a chiral magnetically driven charge-separation difference in collisions of the $^{96}_{44}\mathrm{Ru} + ^{96}_{44}\mathrm{Ru}$ and $^{96}_{40}\mathrm{Zr} + ^{96}_{40}\mathrm{Zr}$ isobars at energies available at the BNL Relativistic Heavy Ion Collider," Phys. Rev. **C98**, 061902 (2018), arXiv:1803.02416 [nucl-ex].

[50] N. N. Ajitanand, Roy A. Lacey, A. Taranenko, and J. M. Alexander, "A New method for the experimental study of topological effects in the quark-gluon plasma," Phys. Rev. **C83**, 011901 (2011), arXiv:1009.5624 [nucl-ex].